Hierarchical Structured Ni Nanoring and Hollow Sphere Arrays by Morphology Inheritance Based on Ordered Through-Pore Template and Electrodeposition

Guotao Duan, Weiping Cai,* Yuanyuan Luo, Zhigang Li, and Yong Lei

Key Lab of Materials Physics, Anhui Key Lab of Nanomaterials and Nanotechnology, Institute of Solid State Physics, Chinese Academy of Sciences, Hefei, 230031 Anhui, People's Republic of China

Received: April 11, 2006; In Final Form: June 20, 2006

Fabrication of micro/nano-hierarchical Ni ordered nanostructured arrays is demonstrated by electrochemical deposition on the ordered alumina through-pore template induced by solution-dipping the colloidal monolayer. The morphology of the Ni nanostructured arrays exhibits a ringlike or hollow spherical structure depending on the template geometry and appropriate deposition parameters. The skeletons of the arrays are of floc- or flakelet-like fine structure on the nanoscale. The formation of such morphologies is attributed to the preferential growth along the inner wall of the alumina pores, while the nanoflakelet fine structure originates from a morphology inheritance process or the transitional product $Ni(OH)_2$ which leads to the final nanostructured Ni crystals. This morphology inherence could be useful in the field of nanofabrication. Such micro/nano-hierarchically structured arrays show good magnetic properties and will find applications in the fields of catalysis, magnetics, optoelectrics, surface-enhanced Raman scattering (SERS), and new nanodevices.

1. Introduction

The nanoring structure has received much attention due to its importance in the fundamental studies of persistent current,[1] the bidomain state in magnetics,[2] and novel optical properties[3] and also due to its technical application in, for example, recording media.[4] The hollow sphere is another special structure with applications ranging from versatile microreactors to advanced functional materials.[5] Generally, nanorings are synthesized by electron-beam lithography,[2] molecular-beam epitaxy,[6] chemical modification,[7] self-assembly,[8] and a suitable structured template technique,[9] while hollow spheres are usually fabricated by templating a colloidal sphere core[10] or a self-assembly strategy.[5b] Such structures and their patterns could be the basis of nanodevice design.[11] However, morphology-controlled synthesis of ordered nanoring-like and hollow spherical-like structured arrays in a simple way is still a challenge.

In recent years, colloidal monolayer lithography has proven to be a promising strategy for the fabrication of various two-dimensional (2D) ordered nanostructured arrays,[12−17] which have exhibited potential applications in nanodevices. Generally, such ordered nanostructured arrays are of compactness in skeleton. Recently, there was a report that showed that when the skeleton is composed of nanosized building blocks or porous structures, the ordered arrays will combine the merits of patterned arrays and nanostructures and show the possibility of application in, for example, surface-enhanced Raman scattering (SERS), superhydrophobicity, and new nanodevices.[18] In this paper, we demonstrate the fabrication of hierarchical Ni nanostructured arrays by electrodeposition based on an ordered Al_2O_3 through-pore template induced by solution-dipping the colloidal monolayer. The Ni arrays show ringlike or hollow spherical structure, depending on the template geometry. Importantly, the skeleton of the arrays is of floc- or flakelet-like fine structure on the nanoscale due to morphology inheritance in the electrochemical process. Such hierarchically structured arrays show good magnetic properties and will find applications in the fields of catalysis, magnetics, optoelectrics, SERS, and new nanodevices. The details are reported in this article.

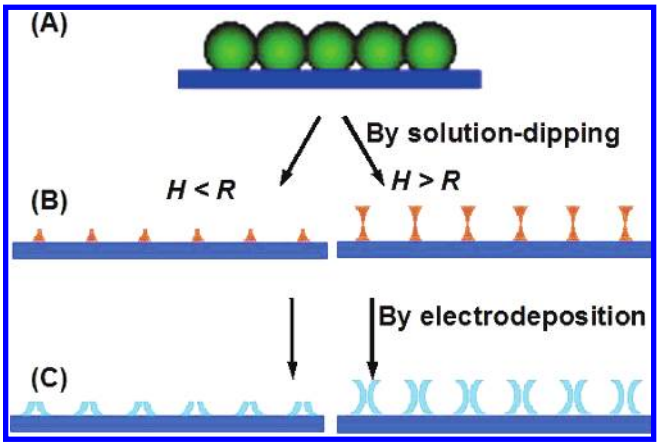

Figure 1. Schematic cross-section illustration of the fabrication procedures for ringlike and hollow spherical-like nanostructured arrays: (A) PS colloidal monolayer on ITO substrate by heating; (B) ordered alumina through-pore array with pore depth (*H*) smaller (left) or larger (right) than the radius of the PS (*R*); (C) ordered Ni ringlike (left) or hollow spherical-like (right) arrays.

2. Experimental Section

The fabrication strategy is illustrated in Figure 1. Some glass slides as substrates were cleaned according to Dyune's procedures.[12a] The suspensions of polystyrene sphere (PS) of 1000 nm in diameter were bought from Alfa Aesar Corporation. Large-area ordered PS colloidal monolayers (larger than 1 cm^2) were synthesized on the glass substrates by spin-coating on a custom-built spin-coater.

Several pieces of ITO-glass substrates were cleaned in acetone, ethanol, and distilled water for 30 min each. The PS monolayer on the glass substrate was integrally lifted off on

* To whom all correspondence should be addressed. E-mail: wpcai@issp.ac.cn.

10.1021/jp062255q CCC: $33.50
Published on Web 07/22/2006

the surface of the distilled water in a cup and then picked up with a piece of ITO glass, as previously illustrated,[13d] followed by heating at 120 °C for 10 min (see step A in Figure 1). In succession, a droplet (~20 μL) of $Al(NO_3)_3$ aqueous solution (with concentrations of 0.2, 0.5, or 1.0 M in this study) was put on the heated monolayer on the ITO-glass substrate, followed by spinning at 300 round per minute to disperse the solution into the interstitials of the PS monolayer, drying at 120 °C for 1 h. Finally, we immersed it into the methylene chloride (CH_2Cl_2) solution to remove the PS monolayer before heating at 150 °C for 8 h to decompose the $Al(NO_3)_3$ into Al_2O_3. After being ultrasonically cleaned in acetone, ethanol, and distilled water for 10 min, respectively, the Al_2O_3 ordered through-pore arrays were thus obtained (see step B in Figure 1).

The substrate coated with the Al_2O_3 through-pore array was used as a working electrode and set into a three-electrode electrolytic cell. An aluminum frame and insulating tape were used to cover the margins of the substrate. A solution composed of 0.01 M $NiCl_2$ and 0.03 M $(NH_4)_2SO_4$ was used as the electrolyte; the pH value was controlled to 8.5 with ammonia. A polycrystalline clean nickel sheet and a saturated calomel electrode (SCE) were used as the auxiliary and reference electrodes, respectively. The distance between the working electrode and the auxiliary electrode was about 6 cm. The electrodeposition was carried out at 60 °C and different deposition potentials versus SCE for a certain time. After deposition, the Al_2O_3 ordered pore skeleton was removed by immersion in 5 wt % NaOH aqueous solution and Ni ordered nanostructured arrays were thus obtained (see step C in Figure 1).

The morphologies of all the samples were examined on a field emission scanning electron microscope (FE-SEM) (Sirion 200). X-ray diffraction (XRD) was performed on a Philips X'Pert instrument using the Cu Kα line (0.154 19 nm). The hysteresis loop measurements of the samples were conducted at 300 and 150 K on a superconducting quantum interference device (SQUID) magnetometer with the applied field parallel to the films.

3. Results and Discussion

3.1. Alumina Ordered Through-Pore Template. On the basis of the PS colloidal monolayer and $Al(NO_3)_3$ solution-dipping,[13c] we can obtain alumina ordered through-pore arrays after removing the PS monolayer. The morphologies can be controlled just by the concentration (C) of $Al(NO_3)_3$. Figure 2 shows typical FE-SEM images of alumina ordered pore arrays on ITO glass with different pore depths (H) corresponding to the colloidal monolayer of 1000 nm PSs. When $C = 0.2$ M, the pores in the arrays are of bowl-like morphology with a pore depth less than the radius (R) of PSs due to the geometry of PSs and show circular openings from the top view (see Figure 2A). When C is up to 0.5 M, $H > R$. A hole in the wall exists between two adjacent pores, resulting from area contact of PSs due to heating the colloidal monolayer before solution-dipping, as seen in Figure 2B. Further characterization shows that the pore wall or skeleton is amorphous Al_2O_3. The formation of alumina ordered through-pore arrays is easily understood. The colloidal monolayer was sintered on the ITO substrate by heating, which led to area contact with the substrate. The ordered through-pore array was thus formed, due to the interstitial geometry in the template, after the $Al(NO_3)_3$ solution-dipping technique and removal of PSs, as previously reported.[13c]

3.2. Ni Nanoring and Hollow Sphere Arrays. On the basis of such Al_2O_3 ordered pore arrays and electrodeposition in the

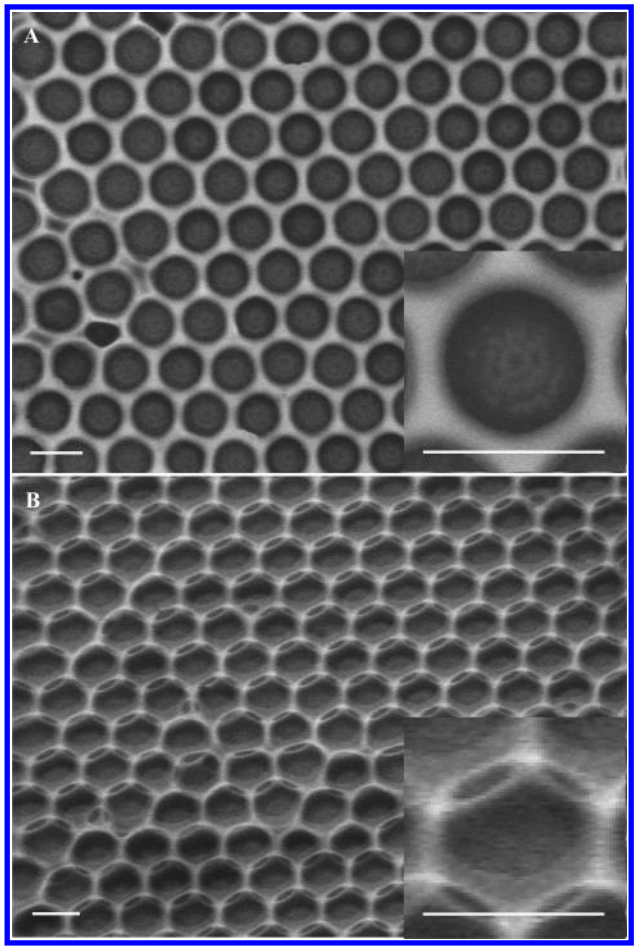

Figure 2. FE-SEM images of ordered alumina through-pore arrays: (A) the array formed with 0.2 M $Al(NO_3)_3$ ($H < R$); (B) the array formed with 0.5 M $Al(NO_3)_3$ ($H > R$). All scale bars are 1 μm.

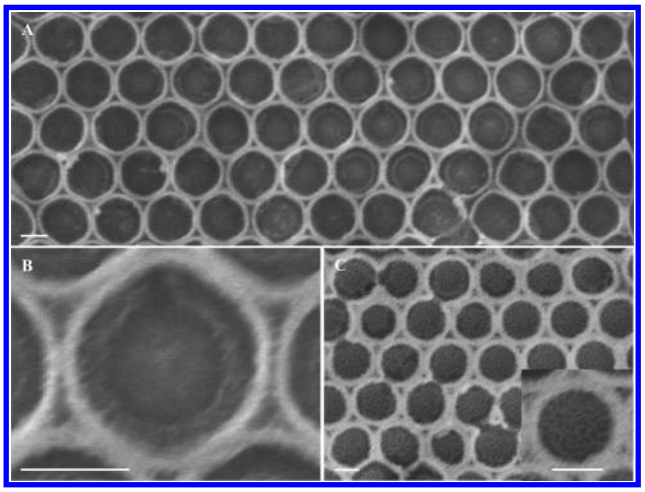

Figure 3. FE-SEM images of ordered Ni nanoring arrays using the template shown in Figure 2A. The electrodeposition potential vs SCE and the deposition time are, respectively, (A) −0.8 V and 20 min and (C) −1.0 V and 16 min. (B) The local enlarged image of sample A. Inset in part C: local enlarged image. All scale bars are 500 nm.

electrolyte, Ni ordered nanostructured patterns were obtained. Figure 3 shows the morphologies of the samples on ITO glass, based on the template shown in Figure 2A, after electrodeposition with different potentials versus SCE and removal of alumina in 5% NaOH solution. At a low negative deposition potential (−0.8 V vs SCE), Ni grows preferentially along the inner wall of the pores, forming a ringlike structure (see Figure 3A,B). The thickness of the film or H value should be close to

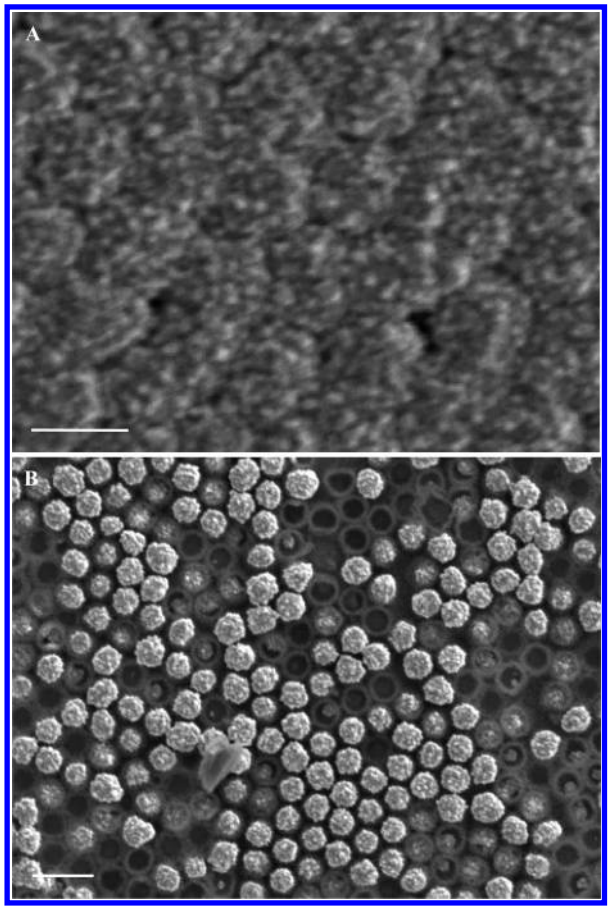

Figure 4. FE-SEM images of ordered Ni arrays using the template shown in Figure 2A. The electrodeposition potential vs SCE and the deposition time are, respectively, (A) −2.0 V and 8 min and (C) −1.2 V and 14 min. The scale bars are 500 nm for part A and 2 μm for part B.

but less than *R*. The high-magnification FE-SEM image shows that there are innumerable floc-like (or flakelet-like) nanocrystals on the ring surface. The morphology of such ordered Ni ringlike arrays can be controlled by the deposition potential. When the deposition potential was −1.0 V versus SCE, the floc-like Ni nanocrystal grew on both the ITO substrate and the inner walls of the pores (see Figure 3C). With further increase of the potential to −2.0 V versus SCE, the floc (or flakelet) vanished, while spherical particles with a rough surface were formed within the ordered alumina pores (see Figure 4A). A middle deposition potential of −1.2 V versus SCE leads to a transitional morphology (see Figure 4B). Both spherical particles and nanorings with flakelet-like structure are formed in or along the pores. The corresponding XRD spectra, shown in Figure 5, indicate that all the as-deposited samples are nickel crystal with a face-centered structure.

As mentioned above, the low negative deposition potential induces the preferred growth of Ni along the pore wall. Thus, if we use the template shown in Figure 2B, truncated hollow spherelike Ni arrays should be obtained by using a low negative deposition potential, which has been confirmed by our further experiments. Figure 6A,B shows the morphology of the sample electrodeposited at −0.8 V versus SCE based on the template shown in Figure 2B, after removal of the template. The circular openings on the top of the hollow spheres can be adjusted by the alumina template morphology which depends on the concentration of the precursor solution $Al(NO_3)_3$. Further, if using the template prepared by 1.0 M $Al(NO_3)_3$, ordered Ni hollow sphere arrays with much smaller top openings were

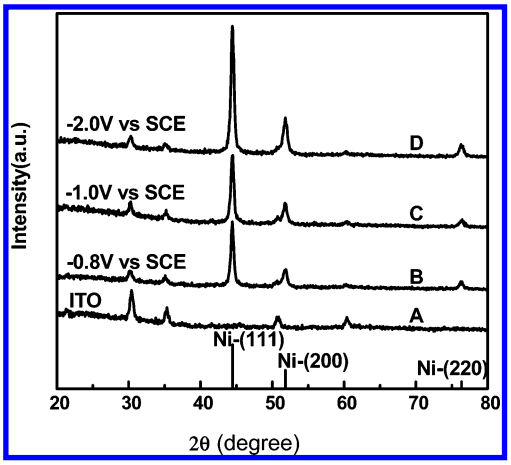

Figure 5. XRD spectra for ITO (A) and the as-deposited samples (B−D), corresponding to Figures 3A,C and 4A, respectively. Bottom: standard diffraction of Ni powers.

obtained after deposition at −0.8 V versus SCE (see Figure 6C). The high-magnification images show that the shell layer of hollow spheres is composed of a large quantity of flakelet-like nanocrystals, which grew along the inner wall of alumina pores, and the thickness of the nanoflakelets is estimated to be nearly 20 nm (see Figure 6B).

Further experiments show that the pH values in the electrolyte and alumina template are important to the morphology of the deposited products, in addition to the deposition potential. A low pH value (say, 4.5) leads to the spherical particle array without flakelet-like fine structure (see Figure 7A). Without the ordered alumina pore array, at low deposition potential (−0.8 V vs SCE), Ni cannot be deposited onto the bare ITO substrate. At −1.0 to −2.0 V versus SCE, the Ni is deposited onto the ITO substrate, forming particle chainlike film without any flakelet-like fine structure (see Figure 7B). As for choice of the alumina as the template, it is crucial to fabricate the Ni arrays with hierachical structure in this work because the transitional product $Ni(OH)_2$ can grow along the pore wall of the alumina (see the following subsection). Alumina is insulating and can be removed in alkaline solution, which is important, since ITO and Ni can be dissolved in acidic solution. Our experiments have demonstrated that ordered pore arrays of many other materials, such as Fe_2O_3, ZnO, TiO_2, CeO_2, and In_2O_3, induced by solution-dipping the colloidal monolayer,[13c] cannot be used as the template for the Ni arrays.

3.3. Formation of Ni Nanostrauctured Arrays. Ni deposition can be described by the following reactions:

$$[Ni(NH_3)_2]^{2+} = Ni^{2+} + 2NH_3 \quad (1)$$

$$Ni^{2+} + 2e^- \rightarrow Ni \qquad (E_1^\circ = -0.23\ V) \quad (2)$$

$$NH_3 + H_2O = NH_4^+ + OH^- \quad (3)$$

$$Ni^{2+} + 2OH^- \rightarrow Ni(OH)_2 \quad (4)$$

$$Ni(OH)_2 + 2e^- \rightarrow Ni + 2OH^- \qquad (E_2^\circ = -0.66\ V) \quad (5)$$

where E° is the standard electrode potential. Ni^{2+} ions in the electrolyte exist in the form of $[Ni(NH_3)_2]^{2+}$,[19] and there are two reaction paths along which deposition of Ni will occur [path I, (1) → (2); path II, (1) → (3) → (4) → (5)]. In an electrolyte with a low pH value, the reaction will go along path I. When the pH is high, the reactions along path II should occur, in

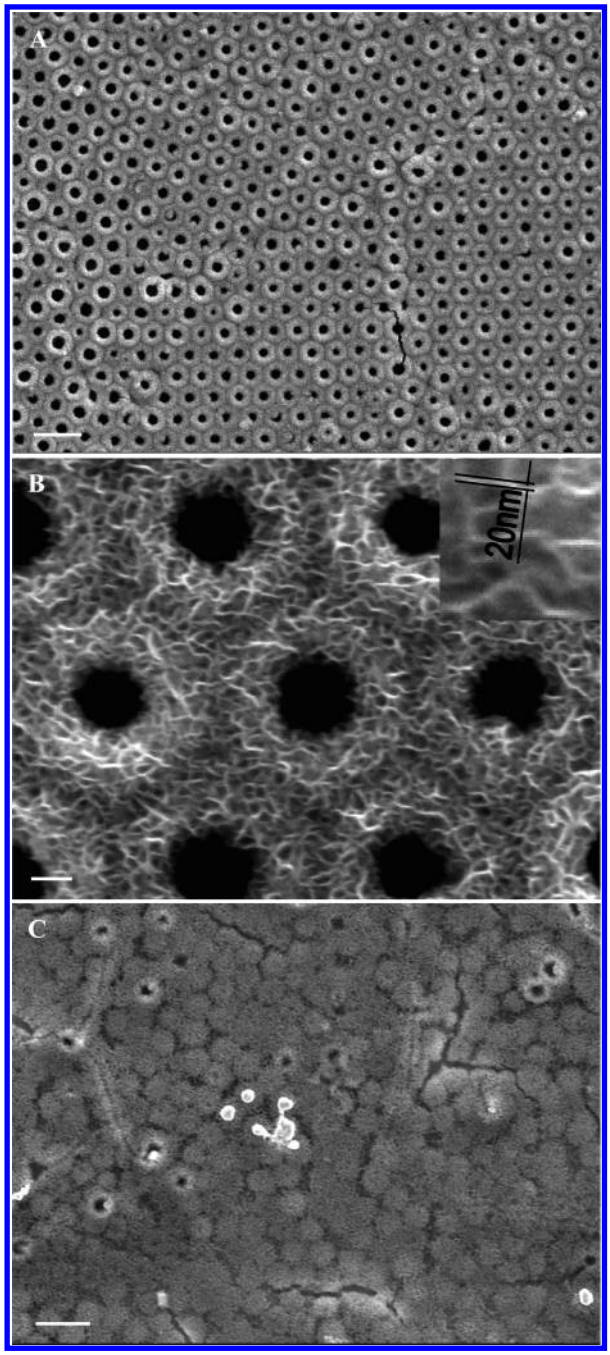

Figure 6. FE-SEM images of the samples electrodeposited at −0.8 V vs SCE based on the ordered alumina templates with $H > R$, prepared by the precursor $Al(NO_3)_3$ with (A) 0.5 M and (C) 1.0 M. (B) The local magnification of part A. The deposition time is 40 min for part A and 50 min for part C. Inset in part B: thickness measurement of the nanoflakelet. The scale bars are 2 μm for parts A and C and 200 nm for part B.

addition to path I. During the initial electrodeposition, the concentration of Ni^{2+} close to the substrate will be increased due to the movement of Ni^{2+} ions to the cathode, which leads to the formation of $Ni(OH)_2$ (see reaction 4) because of high $[OH^-]$. At a low potential, reaction 2 will be restricted and the reaction along path II will thus be dominant. However, when the deposition potential is very high, reaction 2 will be accelerated and the reaction along path I will be dominant again.

In our cases (high pH value and low negative deposition potential), the reaction along path II is dominant. $Ni(OH)_2$ was first formed. As known, $Ni(OH)_2$ is a layered compound of CdI_2 type. Its lamellar 2D structure easily leads to the formation of

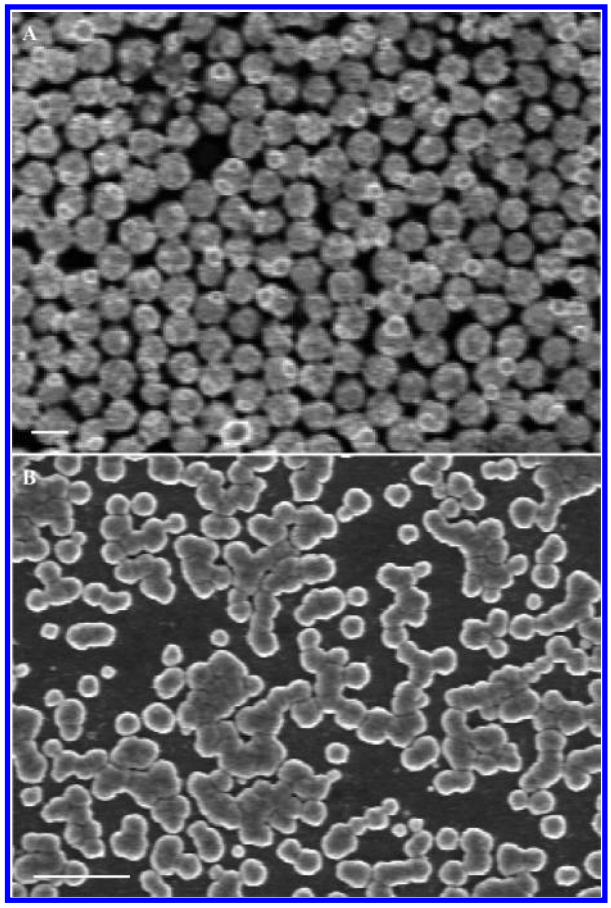

Figure 7. FE-SEM images of sample A electrodeposited at −0.8 V vs SCE for 20 min and at pH 4.5 using the template shown in Figure 2A and Ni particle film (B) electrodeposited at −1.0 V vs SCE for 16 min and at pH 8.5 without template. Both scale bars are 1 μm.

flakelet-like nanocrystals.[20] Thus, deposited $Ni(OH)_2$ would be of flakelet-like fine structure and then decompose into Ni during the reaction, but the flakelet- or floc-like morphology should be kept. We call it a morphology inheritance process.

Then, the formation of ring- or hollow spherelike structure can be understood. Al_2O_3 used here is an insulating material and can be removed easily, which is the main reason that we chose it as the secondary template. When the potential is low negative, corresponding to the reactions along path II, the transitional product $Ni(OH)_2$ preferentially grows along the alumina pore wall because of the low barrier in energy, leading to ringlike or hollow spherelike structured patterns due to the geometry of the Al_2O_3 template. A small increase of the deposition potential can promote growth, resulting in growth along both the pore wall and the ITO substrate after nucleation at the bottom of the pore wall (see Figure 3C).

As mentioned above, a low pH value or high negative deposition potential will lead to the deposition reactions along path I, which results in disappearance of the preferential growth along the pore wall and the flakelet-like fine structure, and spherical particle arrays are formed (see Figures 7A and 4A). In addition, without the Al_2O_3 template, reaction 4 or the reactions along path II will be suppressed and only island-shaped particles without flakelet-like fine structure are formed on the substrate (see Figure 7B). It means that the $Ni(OH)_2$ can nucleate and grow only in the existence of the Al_2O_3 template. Al_2O_3 is crucial and indispensable to get such hierarchically structured patterns.

On these bases, the reactions along path II occur only at a low negative deposition potential, at a high pH value in the

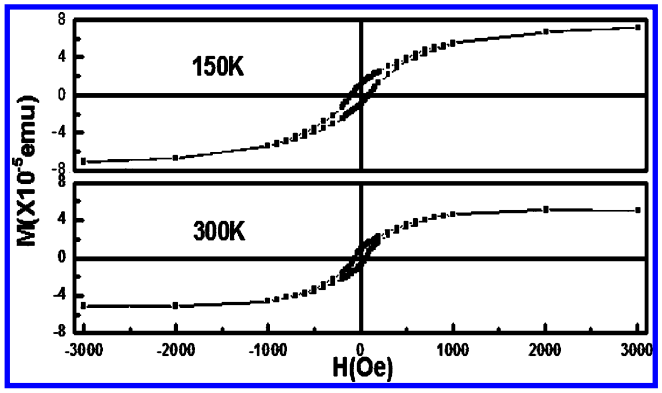

Figure 8. Hysteresis loops for the sample shown in Figure 3A. The applied field is parallel to the film (array) surface.

electrolyte, and with Al_2O_3 template, resulting in the flakelet-like fine structure by morphology inheritance from $Ni(OH)_2$. Otherwise, the reactions along path I will appear, leading to the final morphology of spherical particles. Thus, in this case, the reactions along paths I and II should coexist at high pH value in the electrolyte and with Al_2O_3 template but at a moderate deposition potential. This has been confirmed by our experiment, as shown in Figure 4B, which corresponds to the potential −1.2 V versus SCE and the template ($H < R$) shown in Figure 2A. Both spherical particles and nanorings with flakelet-like structure are formed, which should originate from the reactions along paths I and II, respectively.

As for the occurrence of reaction 5, because the deposition potentials used in our case are more negative than $E_2°$ (−0.66 V), reaction 5 is feasible from a thermodynamical point of view, since the $Ni(OH)_2$ can be formed on the alumina wall at a high pH value.

3.4. Magnetic Measurements. Such hierarchical structured Ni nanoring or hollow sphere arrays exhibit ferromagnetic behaviors, as shown in Figure 8, corresponding to the Ni nanoring array shown in Figure 3A (it is similar to the hollow sphere arrays). There is a hysteresis loop with a coercivity of 63 Oe at 300 K and 96 Oe at 150 K. Commonly, Ni nanocrystals below a critical size (35 nm at 300 K) should manifest superparamagnetism with no hysteresis due to the thermal fluctuation of spin.[20] Although the ultrathin nanoflakelets in our case are less than 35 nm in size, it shows the significant hysteresis even at room temperature. X-ray photoemission spectroscopy analysis has confirmed that Ni nanoflakelets are of some surface oxidation. The hysteresis in our case could be attributed to such surface oxidation, since NiO shells can isolate each Ni core and the exchange interaction at the Ni/NiO interface may fix the spin of the Ni core.[21] It should be mentioned that the formation of the NiO shell is induced by exposure to the air after preparation of the sample, instead of dehydration of $Ni(OH)_2$, which cannot lead to the Ni/NiO core/shell structure.

4. Summary and Remarks

In conclusion, we have demonstrated the fabrication of hierarchical Ni ordered nanostructured arrays by morphology inheritance in an electrochemical process based on an ordered Al_2O_3 through-pore template induced by solution-dipping the colloidal monolayer. In the electrolyte with a high pH value, deposition on the substrate with Al_2O_3 template at a low negative potential will lead to the formation of the transitional product $Ni(OH)_2$, which is of flakelet-like fine structure and which will then decompose into Ni with similar morphology during the reaction. The ringlike or hollow spherical-like Ni ordered nanostructured arrays with the fine structure are thus obtained, depending on the pore geometry of the alumina template. Such hierarchical nanostructured Ni arrays are expected to combine the merits of both patterned arrays and nanocrystals. They could exhibit some new properties and potential applications in, for example, (1) magnetics or magnetic nanodevices; (2) SERS (Ni has proven to be an effective SERS active material with the enhancement factor correlated to its surface geometry,[22] and the hierarchical structures in our case could be of high enhancement factor due to their periodic geometrical characteristics and nanosized flakelets which both are beneficial to the SERS effect[18a,23]); (3) catalysis, hydrogen-store materials, or films due to the ultrathin nanoflakelets with high surface area; and (4) new functional nanodevices.

Acknowledgment. This work was supported by the National Natural Science Foundation of China (Grant No. 10504035) and the Major State research program of China "Fundamental Investigation on Micro-Nano Sensors and Systems based on BNI Fusion" (Grant No. 2006CB300402).

References and Notes

(1) Matveev, K. A.; Larkin, A. I.; Glazman, L. I. *Phys. Rev. Lett.* **2002**, *89*, 096802.
(2) Rothman, J.; Kläui, M.; Lopez-Diaz, L.; Vaz, C. A. F.; Bleloch, A.; Bland, J. A. C.; Cui, Z.; Speaks, R. *Phys. Rev. Lett.* **2001**, *86*, 1098.
(3) Aizpurua, J.; Hanarp, P.; Sutherland, D. S.; Käll, M.; Bryant, G. W.; Abajo, F. *Phys. Rev. Lett.* 2003, *90*, 057401.
(4) Li, S. P.; Peyrade, D.; Natali, M.; Lebib, A.; Chen, Y.; Ebels, U.; Buda, L. D.; Ounadjela, K. *Phys. Rev. Lett.* **2001**, *86*, 1102.
(5) (a) Caruso, F. *Chem.—Eur. J.* **2000**, *6*, 413. (b) Hu, Y.; Jiang, X.; Ding, Y.; Chen, Q.; Yang, C. *Adv. Mater.* **2004**, *16*, 933.
(6) Warburton, R. J.; Schäflein, C.; Haft, D.; Bickel, F.; Lorke, A.; Karrai, K.; Garcia, J. M.; Schoenfeld, W.; Petroff, P. M. *Nature* **2000**, *405*, 926.
(7) Sano, M.; Kamino, A.; Okamura, J.; Shinkai, S. *Science* **2001**, *293*, 1299.
(8) Li, F.; Dong, Y.; Gao, P.; Xin, X.; Wang, Z. *Angew. Chem., Int. Ed.* **2004**, *43*, 5238.
(9) (a) Hobbs, K. L.; Larson, P. R.; Lian, G. D.; Keay, J. C.; Johnson, M. B. *Nano Lett.* **2004**, *4*, 167. (b) Pearson, D. H.; Tonucci, R. J.; Bussmann, K. M.; Bolden, E. A. *Adv. Mater.* **1999**, *11*, 769.
(10) (a) Imhof, A. *Langmuir* **2001**, *17*, 3579. (b) Tartaj, P.; González-Carreño, T.; Serna, C. J. *Adv. Mater.* **2001**, *13*, 1620.
(11) (a) Huang, Y.; Duan, X. F.; Wei, Q. Q.; Lieber, C. M. *Science* **2001**, *291*, 630. (b) Liu, B.; Zeng, H. C. *J. Am. Chem. Soc.* **2004**, *126*, 16744.
(12) (a) Haynes, C. L.; Van Duyne, R. P. *J. Phys. Chem. B* **2001**, *105*, 5599. (b) Ghanem, M. A.; Bartlett, P. N.; Peter de Groot; Zhukov, A.; *Electrochem. Commun.* **2004**, *6*, 447.
(13) (a) Che, X.; Chen, Z.; Fu, N.; Lu, G.; Yang,B. *Adv. Mater.* **2003**, *15*, 1413. (b) Bartlett, P. N.; Baumberg, J. J.; Coyle, S.; Abdelsalam, M. E. *Faraday Discuss.* **2004**, *125*, 117. (c) Sun, F.; Cai, W.; Li, Y.; Cao, B.; Lei, Y.; Zhang, L. *Adv. Funct. Mater.* **2004**, *14*, 283. (d) Sun, F.; Cai, W.; Li, Y.; Cao, B.; Lu, F.; Duan, G.; Zhang, L. *Adv. Mater.* **2004**, *16*, 1116.
(14) (a) McLellan, J. M.; Geissler, M.; Xia, Y. *J. Am. Chem. Soc.* **2004**, *126*, 10830. (b) Yi, D. K.; Kim, D. Y. *Nano Lett.* **2003**, *3*, 207.
(15) Chen, Z.; Zhan, P.; Wang, Z.; Zhang, J.; Zhang, W.; Ming, N.; Chan, C.; Sheng, P. *Adv. Mater.* **2004**, *16*, 417.
(16) Kuo, C.; Shiu, J.; Chen, P. *Chem. Mater.* **2003**, *15*, 2917.
(17) Huang, Z. P.; Carnahan, D. L.; Rybczynski, J.; Giersig, M.; Wang, D. Z.; Wen, J. G.; Kempa, K.; Ren, Z. F. *Appl. Phys. Lett.* 2003, *82*, 460.
(18) (a) Lu, L.; Randjelovic, I.; Capek, R.; Gaponik, N.; Yang, J.; Zhang, H.; Eychmüller, A. *Chem. Mater.* **2005**, *17*, 5731. (b) Li, Y.; Cai, W.; Duan, G.; Cao, B.; Sun, F.; Lu, F. *J. Colloid Interface Sci.* **2005**, *287*, 634.
(19) Natarajan, C.; Matsumoto, H.; Nogami, G. *J. Electrochem. Soc.* **1995**, *144*, 121.
(20) Wang, D.; Song, C.; Hu, Z.; Fu, X. *J. Phys. Chem. B* **2005**, *109*, 1125.
(21) Seto, T.; Akinaga, H.; Takano, F.; Koga, K.; Orii, T.; Hirasawa, M. *J. Phys. Chem. B* **2005**, *109*, 13403.
(22) Tian, Z.; Ren, B.; Wu, D. *J. Phys. Chem. B* **2002**, *106*, 9463.
(23) (a) Gaponenko, S. G. *Phys. Rev. B* **2002**, *65*, 140303R. (b) Kreibig, U.; Vollmer, M. *Optical Properties of Metal Clusters*; Springer-Verlag: New York, 1995.